Supplement to: Microwave Near-Field Imaging of Two-Dimensional Semiconductors

Samuel Berweger,[*,†] Joel C. Weber,[†] Jimmy John,[‡] Jesus M. Velazquez,[‡] Adam Pieterick,[‡] Norman A. Sanford,[†] Albert V. Davydov,[¶] Bruce Brunschwig,[‡] Nathan S. Lewis,[‡] Thomas M. Wallis,[†] and Pavel Kabos[†]

National Institute of Standards and Technology, Boulder, CO, 80305, Kavli Nanoscience Institute, Beckman Institute, Joint Center for Artificial Photosynthesis, and Department of Chemistry and Chemical Engineering, Caltech, Pasadena, CA, 91125, and National Institute of Standards and Technology, Gaithersburg, MD, 20899

E-mail: samuel.berweger@nist.gov

Comparison of S_{11} and S'_{11}

As noted in the manuscript we preferably use the $S'_{11} = \frac{dS_{11}}{dV}$ data channel as opposed to the raw S_{11} signal, primarily due to the robustness of S'_{11} (as all values here are complex unless otherwise noted, the tilde has been dropped). Shown in Figure S1 is a comparison of these data channels. Figure S1(a-b) shows the raw and unprocessed S'_{11} data, corresponding to the $V_b = 0$ V image in Figure 2 (real and imaginary components are calculated from the amplitude and phase channels acquired). The S'_{11} signal remains stable, showing little drift in either signal or noise. In contrast, the simultaneously acquired unprocessed S_{11} channels (c,d) show significant drift in both amplitude

[*]To whom correspondence should be addressed
[†]NIST Boulder
[‡]Caltech
[¶]NIST Gaithersburg

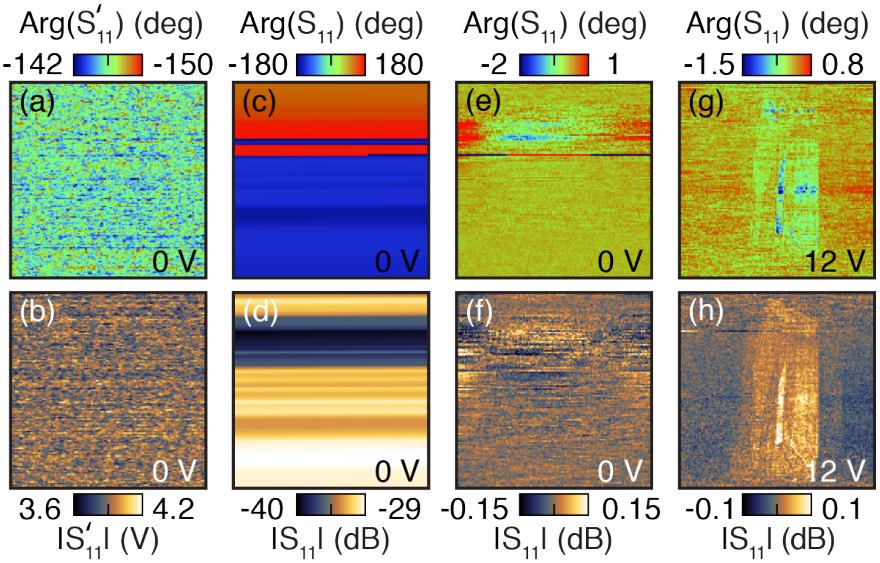

Figure S1: Comparison of S_{11} and S'_{11} data channels. Unprocessed data channels showing raw S'_{11} (a,b), and S_{11} (c,d) from the $V_b = 0$ V scan shown in Figure 2(b). Processed scans from (c,d) after line-fitting are in (e,f), showing residual signal drift and high noise. S_{11} scan acquired with $V_b = 12$ V (g,h) after line-fitting procedure.

and phase. The corresponding S_{11} images after post-processing using line-by-line subtraction to eliminate the long-term drift still show significant fluctuations in signal as well as noise (e,f). Although contrast is seen, compared to the S'_{11} channel (Figure 2), the S_{11} image at $V_b = 12$ V still suffers from signal drift and high noise (g-h).

The observed signal drift and variations in noise are particularly detrimental to S_{11}-voltage sweeps. While long term drift can typically be corrected in raster-scanned images as shown, drift renders S_{11}-voltage sweeps unusable. We have not established the origin of this drift, but we assume it arises from thermal fluctuations of the coaxial transmission line and circuit elements.

Signal Reproducibility

Streaking is seen in the SMM images shown in Figure 3 due to contamination of the tip-sample junction by residual soft matter on the sample surface, leading to an increase in the contact resistance and associated reduction in the SMM signal. Shown in Figure S2 are additional scans of the same crystals shown in Figure 3. Figure S2(a) and (c) shows scans of the same sheet as Fig-

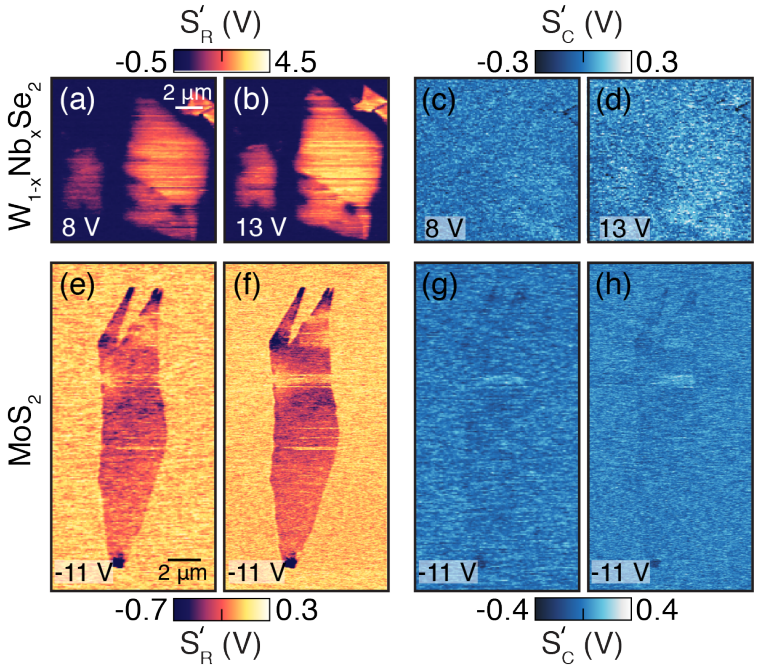

Figure S2: Repeat scans of the crystals in Figure 3 showing the reproducibility of the SMM data.

ure 3(a) (shown here in b and d), with tip biases as indicated. Similarly, Figure S2(e) and (g) show repeat scans of the same region as Figure 3(b) (shown here in f and h). From the MoS_2 crystal it can be seen that spatial variations in signal intensity as well as their strengths are quantitatively reproducible. Some streaking is observed; it is often reproducible and correlated with large surface defects that likely contaminate the tip sample contact and increase the contact resistance. However, this effect is typically spatially limited only to lines where tip passes over such defects. This shows that the tip-sample junction is highly robust and contamination is rapidly removed through mechanical friction during scanning.

For the case of the $W_{1-x}Nb_xSe_2$ weaker streaking is observed accounting for typical signal changes <25%. Thus, while some degree of tip-sample contact contamination is observed, the scan remains robust and significant spatial variations are reproducible, as is the effect of localized defects and the transition between layer thicknesses. Despite streaking, the SMM signal remains reproducible, with the reduced signal strength at V_b = 8 V as expected. For S′-Voltage sweeps we initially ensure that the tip-sample junction is not contaminated, and minimize subsequent contamination by lifting the tip between points. We note that despite signal variations, the bias-

dependence of the SMM signal remains, indicating that the tip-sample contact remains conductive.

Origin of contrast

Here we describe the origin of our measured signal. The measured reflected microwave signal is given by

$$S_{11} = \frac{Z_L - Z_0}{Z_L + Z_0} = \frac{Y_0 - Y_L}{Y_0 + Y_L}, \tag{1}$$

with the 50 Ω reference load Z_0, load Z_L, and the admittance $Y = \frac{1}{Z} = \frac{1}{R_{\mathrm{TMD}}} + i\omega C_{\mathrm{TMD}}$. We use a shunt resistor and phase shifter to impedance match the load to the reference load, and thus $Z_L \approx Z_0 = 50\ \Omega$. Furthermore, as V_b is only applied at the tip, $Y_0' = 0$, and therefore we can approximate

$$S_{11} \approx -\frac{Y_L}{2Y_0} \propto -Y_L \quad \text{and} \quad S_{11}' \approx -\frac{Y_L'}{2Y_0} \propto -Y_L'. \tag{2}$$

Based on the lumped element model in Figure S3(a) we then have $S_{11} \propto -(Y_{\mathrm{str}} + Y_s)$ and $dS_{11}/dV = S_{11}' \propto -(Y_{\mathrm{str}}' + Y_s')$.

Ultimately we want to determine the relationship between Y_{TMD}' and the measured signal. Shown in Figure S3(b) is a S_{11}'-voltage sweep, the difference between a sweep acquired with the tip retracted $\sim$6 μm from the sample and in feedback on the support substrate. Due to the short range of the near-field tip-sample interaction, the lack of a distance-dependent signal change indicates that $Y_{sub}' = \frac{d}{dV}\left(\frac{Y_{SiO_2} Y_{Si}}{Y_{SiO_2} + Y_{Si}}\right) = 0$. There is also a lack of metal-insulator-semiconductor junction behavior. While band-bending due to the p^{++}-doped Si substrate is expected to result in a bias-dependent signal, it is likely that the signal is dominated by the SiO_2 sheet and associated surface charges. It is important to note that while $Y_{sub}' = 0$, $Y_{sub} \neq 0$.

The lack of Si response provides a facile means for background-subtraction. We have ascertained that the signal measured on the support substrate originates only from the stray admittance $S_{11,\mathrm{SiO_2}}' \propto -(Y_{\mathrm{str}}' + Y_{sub}') = -Y_{\mathrm{str}}'$. Subtracting the signal from the support substrate from that ac-

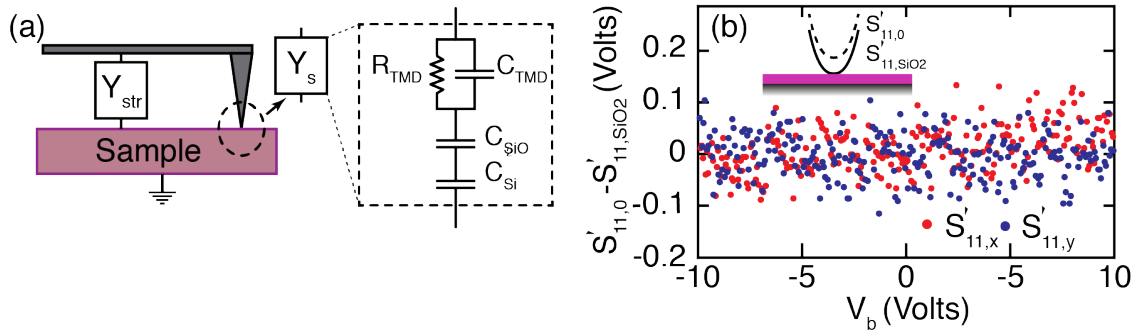

Figure S3: (a) Schematic of lumped element model of experiment. (b) S'_{11} as a function of tip bias, shown as the difference between sweeps taken with the tip retracted by ~6 μm ($S'_{11,0}$) and with the tip in feedback on SiO_2 adjacent to a TMD patch (S'_{11,SiO_2}).

quired on the TMD layer directly yields the sample response

$$S' \equiv S'_{11,SiO_2} - S'_{11,TMD} \propto Y'_s. \tag{3}$$

Lastly, we note that the sample response $Y'_s = \frac{d}{dV}\left(\frac{Y_{TMD}Y_{sub}}{Y_{TMD}+Y_{sub}}\right)$ reduces to $Y'_s = Y'_{TMD}$ for $Y'_{sub} = 0$ and $Y_{sub} \gg Y_{TMD}$. This assumption holds for small values of the sample conductivity and is largely valid over the values studied here.

The experimentally measured S'_{11} signal can therefore readily be interpreted in terms of the TMD substrate response. This underscores one key advantage posed by the derivative signal compared to the reflection signal S_{11}: the lack of response from the support substrate enables straightforward extraction of the TMD response.

Conductive Contact

As noted in the manuscript our experimental S'–voltage sweeps strongly suggest a primarily resistive tip–sample junction that enables carrier transport. Shown in Figure S4 are the experimental $S_{11,R} = \int S'_R \, dV$ for WSe_2 and $W_{1-x}Nb_xSe_2$ as calculated from Figure 5 of the manuscript. Of note is that both curves increase with positive bias despite doping with carriers of opposite charge, and that the signal is primarily in the resistive data channel. Dashed lines are illustrations of the

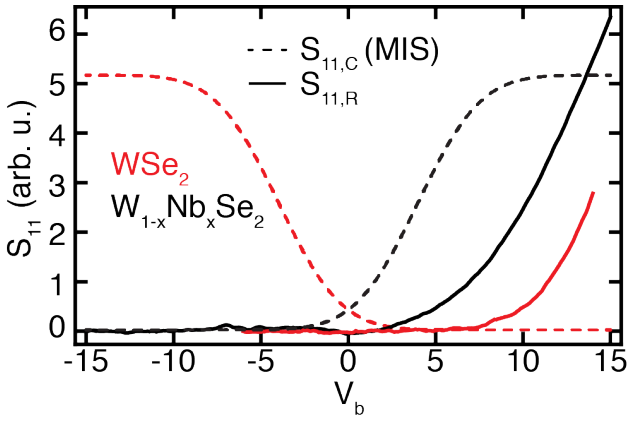

Figure S4: Comparison of measured $S_{11,R}$ as calculated from Figure 5 in main text (solid lines) and qualitative $S_{11,C}$ curve based on conventional MIS junction.

expected $S_{11,C}$ behavior based on a metal-insulator-semiconductor (MIS) junction with a Schottky barrier.[1] For the case of a MIS junction, the capacitance is expected to decrease with carrier inversion, as indicated. For the oppositely doped materials, the $S_{11,C}$ and S'_C contrast is expected to increase at opposite values of the tip bias, in contrast to what is observed.

The large difference between the behavior observed here and the expected $S_{11,C}$-voltage characteristics of a capacitive tip-TMD junction strongly suggest a contact with little or no capacitance compontent. Furthermore, the signal quality and robustness typically increases with increasing AFM setpoint (higher tip pressure on sample) and deposition of 3 nm of Al_2O_3 by atomic layer deposition drastically changed the nature of the SMM signal, further supporting this conclusion. While our analysis (see below) suggests a resistive contact, we cannot rule out a small Schottky barrier which may be overcome in part due to thermionic emission facilitated by ohmic heating.

Model Details

Theoretical simulations were performed with finite element analysis using COMSOL 4.2 using methodologies previously used to simulate SMM measurements from 2D materials.[2–5] With the size of our system significantly smaller than the free-space wavelength ($\lambda = 15$ cm at 2 GHz) the quasistatic approximation holds and we use the AC/DC module. We use a radially symmetric

geometry (axisymmetry) to optimize computation time, and reproduce the experimental geometry with a 260 nm oxide layer ($\varepsilon = 3.9$) on degenerately boron doped Si ($n = 10^{19}$ cm^{-1}, $\sigma = 10^4$ S/m, $\varepsilon = 11.9$). The 3D TMD layer was placed in electrical contact with the Pt tip (tip-sample resistance 50 Ω unless otherwise indicated), with a thickness of 0.65 nm chosen to correspond to commonly accepted values.[6] In order to ensure a sufficiently fine mesh for the TMD sheet we verified that our mesh thickness of 3 yielded identical results to a thickness of 2. A TMD in-plane dielectric constant $\varepsilon = 7$[7] was used, although as previously noted,[2] the SMM signal depends only weakly on the TMD dielectric constant, but rather is determined primarily by the conductivity.

Tip-Sample Contact Conductivity Variations

While the reproducibility observed in our measurements suggests a conducting contact with a low contact resistance, observed streaking is due contamination of the sample-contact by, e.g., residual exfoliation adhesive. Here we show the effect of an increase in the contact resistance on the SMM signal response. We further explore the influence of conductivity variations across the TMD as it may arise due to, e.g., band bending in the immediate vicinity of the tip.

We first examine the effect of changes in the tip-sample resistance on the SMM signal. Shown in Figure S5(a) are the conductivity-dependent resistive and capacitive components of the microwave admittance for tip-sample resistances as shown. With the curve for 1 Ω almost identical to and obscured by the 1 kΩ curve this shows that the SMM signal is robust to changes in tip-

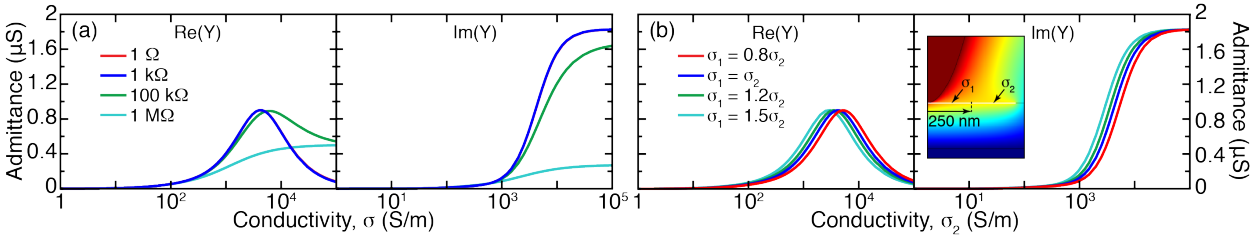

Figure S5: Conductivity-dependent resistive and capacitive components (a) of the admittance at the experimental microwave frequency (2.4 GHz) with varying tip-sample contact resistance. Note that curves for 1 Ω and 1 kΩ are nearly identical with the former obscured by the latter. The influence of an inhomogeneous sample conductivity (b) in the immediate vicinity of the tip.

sample resistance for small values, with notable deviations only appearing for 100 kΩ. The SMM signal is seen to change drastically for $R_t = 1$ MΩ, where the tip-sample interaction transitions to one dominated by capacitive near-field coupling. In particular, the capacitive coupling regime is expected to show MIS behavior, which strongly suggests that variations in tip-sample resistance remain in the $\lesssim 100$ kΩ range. The signal streaking seen with the tip passing over large defects (Figure S2) typically results in little or no signal due to very large resistance changes. This conclusion is further supported by the increase in S'_C seen during streaking in Figure S2(g,h), which is indicative of transition into the capacitive interaction regime. Thus, the signal variations seen from streaking on, e.g., the $W_{1-x}Nb_xSe_2$ sample, suggests smaller tip-sample resistance changes on the order of < 100 kΩ.

We assume homogeneous sample conductivities throughout our simulations, but variations may exist due to band bending and associated charge accumulation in the immediate vicinity of the tip, as well as poor charge equilibration over the sheet at low conductivities approaching the insulating limit. While we are not sensitive to variations at very low conductivities ($\ll$1 S/m) due to our sensitivity limit of $\approx$100 S/m, we explore here the effect of variations in the vicinity of the tip. We approximate possibly more complex spatial profiles by two distinct regions of the sample with differing conductivities. Shown in Figure S5(b) are the conductivity-dependent resistive and capacitive signal components of the microwave admittance for spatially varying conductivity across the TMD sheet as shown in the inset. It is seen that a varying local conductivity near the tip shifts the resonant-type behavior to lower conductivities for increasing relative conductivity. We note that apart from the conductivity peak of the resonance-type curves, they remain identical in shape and amplitude. While more intricate conductivity variations may have more complex effects, this behavior is independent of sheet size and strongly suggests that spatial conductivity variations would have little or no effect on our data interpretation and fitting, and would primarily influence the estimate of the zero-bias conductivity and doping.

References

(1) Sze, S. M.; Ng, K. K. *Physics of Semiconductor Devices*; Wiley, 2007.

(2) Liu, Y.; Ghosh, R.; Wu, D.; Ismach, A.; Ruoff, R.; Lai, K. *Nano Lett.* **2014**, *14*, 4682.

(3) Kundhikanjana, W.; Lai, K.; Wang, H.; Dai, H.; Kelly, M. A.; Shen, Z. X. *Nano Lett.* **2009**, *9*, 3762.

(4) Tselev, A.; Lavrik, N. V.; Vlassiouk, I.; Briggs, D. P.; Rutgers, M.; Proksch, R.; Kalinin, S. V. *Nanotechnol.* **2012**, *23*, 385706.

(5) Lai, K.; Kundhikanjana, W.; Kelly, M.; Shen, Z. X. *Rev. Sci. Instrum.* **2008**, *79*, 063704.

(6) Radisavljevic, B.; Radenovic, A.; Brivio, J.; Giacometti, V.; Kis, A. *Nat. Nanotech.* **2011**, *6*, 147.

(7) Molina-Sánchez, A.; Wirtz, L. *Phys* **2011**, *84*, 155413.